actuators

Article

Optimal Voltage Distribution on PZT Actuator Pairs for Vibration Damping in Beams with Different Boundary Conditions

Andrea Rossi * and **Fabio Botta**

Department of Industrial, Electronic and Mechanical Engineering, Roma Tre University, Via Vito Volterra 62, 00146 Rome, Italy
* Correspondence: andrea.rossi@uniroma3.it; Tel.: +39-06-5733-3559

Abstract: In recent decades, many studies have been conducted on the use of smart materials in order to dampen and control vibrations. Lead zirconate titanate piezoceramics (PZT) are very attractive for such applications due to their ability of delivering high energy strain in the structure. A pair of piezoelectric actuators can actively dampen the resonances of the structure, but the damping effectiveness strongly relies on its location. Damping effectiveness can be substantially increased if the structure is fully covered with PZT actuator pairs and the voltage distribution on each pair is optimized. In this way, each actuator pair contributes to the vibration attenuation and only the driving voltage's sign, distributed on each actuator pair, needs to be identified for each resonance. This approach is here applied to the case of Euler–Bernoulli beams with constant cross-section and the optimal voltage distribution is investigated for several boundary conditions. The theoretical model results were corroborated with finite element simulations, which were carried out considering beams covered by ten PZT actuator pairs. The numerical results agree remarkably well with the theoretical predictions for each examined case (i.e., free-free, pinned-pinned, and fixed-fixed).

Keywords: piezoelectric; vibration; beam; damping

Citation: Rossi, A.; Botta, F. Optimal Voltage Distribution on PZT Actuator Pairs for Vibration Damping in Beams with Different Boundary Conditions. *Actuators* **2023**, *12*, 85. https://doi.org/10.3390/act12020085

Academic Editor: André Preumont

Received: 24 January 2023
Revised: 12 February 2023
Accepted: 14 February 2023
Published: 16 February 2023

1. Introduction

Resonance in flexible structures may threaten their safe operation if the structural damping is inadequate to prevent the fatigue limit from being exceeded. As a result, many passive and active damping systems have been developed by designers since the second half of the 1900s. The growing need for lightweight and high-strength components has promoted the development of smart materials that can modulate some structure's mechanical characteristics, whether environmental circumstances make it necessary. The behaviour of these materials can be tuned through the application of external stimuli such as temperature [1,2], electric field [3], magnetic field [4,5], etc. Among the available smart materials, the most suitable is lead zirconate titanate (PZT) for damping, vibration control, and energy harvesting applications [6–8]. Indeed, they can induce high strain energy, exhibit wide bandwidth, and fast stimulus response, which make them very attractive for sensor and actuator operation.

However, piezoceramics have been implemented in several applications such as: energy harvesting [6], micro-actuators for subspace aircraft [9], wings actuation in drones [10], vibration damping in cantilever beam under support motion [11], turbomachinery blades vibration [12–15], axial compressor vibration damping [16], rotating plates vibration control [17], and active fan blades vibration [18,19].

Active piezoelectric damping systems are usually superior to passive ones because the behaviour of the actuators can be tailored to the excitation of each eigenmode. The efficiency of these systems is considerably determined by the positioning of the PZT actuators on the structure. Former investigations regarding the optimal piezoelectric positioning to efficiently damp single mode excitationwere performed by Refs. [20,21]. Barboni et al. [22]

showed that a single PZT actuator must be positioned among two consecutive zero curvature points in order to excite a bending mode in an Euler–Bernoulli beam. This method was proposed for cantilever, simply supported and pinned-fixed boundary conditions. This kind of optimization criterion is referred to as the maximization of the structure transverse deflection [23]. The vertical displacement of the beam is considered to identify the optimal length and position of piezoelectric actuators pair. Given that the vertical displacement is provided by flexural actions such as the bending moments provided by the piezoelectric actuators, then the optimization depends on the partial derivative of the mode shapes with respect to the beam length [24]. The optimal placement of a single PZT pair to control single and bi-modal excitations in cantilever beams was proposed by Refs. [25,26].

In 2018, a new technique was proposed for optimising the efficiency of active systems based on PZT actuator pairs (PPs) bonded onto cantilever beams [27]. In this method, the PZT pairs are always activated regardless of the excited mode. It was shown that, if the voltage that has to be supplied on each electrode of every actuator pair is optimised, then the achievable damping is much higher than using a single optimally positioned PZT pair on a cantilever beam.

In this paper, the optimal voltage distribution approach is applied to the case of Euler–Bernoulli beams with constant cross-section and investigated for several boundary conditions. The free-free, pinned-pinned, and fixed-fixed boundary conditions were considered in order to offer the possibility of gaining insight into the best voltage distributions in case of resonance, which may be appealing for designers of PZT-based damping systems. For example, free-free beam dynamics is often used to study vibrations in several sports equipment such as tennis racquets [28], baseball bats [29], etc. The dynamic behaviour of turbomachinery stator blades can be modelled as fixed-fixed beams, while the pinned-pinned beam model is often adopted in several civil, aircraft, and mechanical engineering applications [30].

From the dynamics of the Euler–Bernoulli beam, a theoretical model is presented to identify the optimal voltage distribution on PZT actuator pairs that entirely cover the structure. The reliability of the theoretical model was proven by means of finite element method (FEM) simulations. The numerical results reveal a fair agreement with the analytical predictions, confirming the accuracy of the theoretical model.

In the following Sections, the theoretical model for the identification of the optimal voltage distribution on PZT actuator couples is described in Section 2. The numerical model and outcomes are reported and discussed in Section 3.

2. Optimal Voltage Distribution on Piezoelectric Actuators Coupled with Beams under Different Constraints

In Figure 1, the beams coupled with piezoelectric actuator pairs are depicted for the considered boundary conditions.

The equilibrium equation of the beam can be obtained through the principle of virtual work:

$$\delta L_e = \delta L_i + \delta L_a + \delta L_p \tag{1}$$

where the δL_e, δL_i, δL_a, and δL_p represent, respectively, the virtual works of elastic, inertial, external, and piezoelectric forces. In this paper, the focus will be on flexural vibrations, so that, if w represents the vertical displacement of the beam section the virtual works can be written in the form (the superimposed tilde indicates the virtual quantities):

$$\begin{cases} \delta L_e = \int_0^L M_e(x,t)\, \tilde{w}''(x,t)dx \\ \delta L_i = -\int_0^L \rho A\, \ddot{w}(x,t)\, \tilde{w}(x,t)dx \\ \delta L_a = \int_0^L f_a(x,t)\, \tilde{w}(x,t)dx \end{cases} \tag{2}$$

where $M_e(x,t) = EIw''(x,t)$ is the internal elastic moment while $f_a(x,t)$ is the external force.

By distributing the voltage on the PZT plates as reported in Figure 2, the actions exerted on the beam by each pair of actuators can be represented by a pair of bending moments $M_p(t)$ applied to their ends.

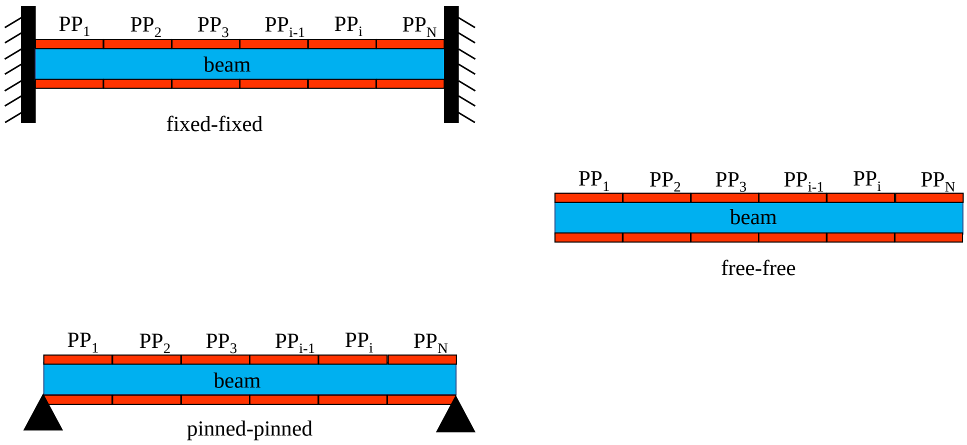

Figure 1. Beams coupled with PZT actuator pairs (PPs) for different boundary conditions: free-free, fixed-fixed, and pinned-pinned.

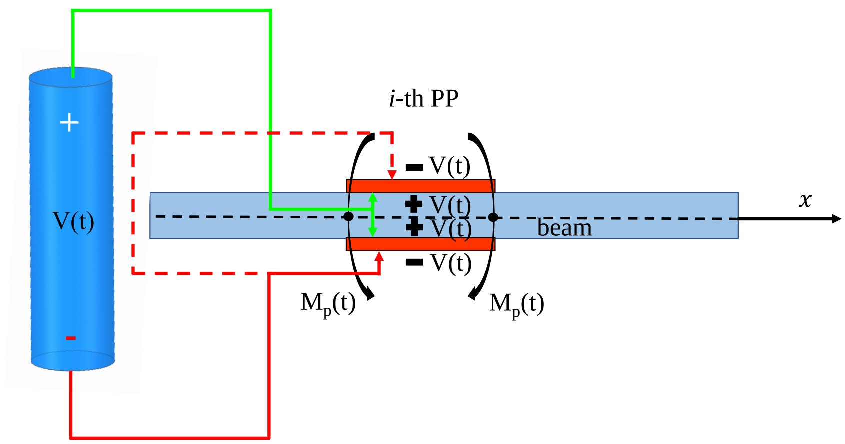

Figure 2. *i*-th PZT actuator pair actions induced on the beam.

Denoting with:

$$\begin{cases} \Lambda(t) = \frac{d_{31}}{T_a} V(t) \\ \psi = \frac{E_b T_b}{E_a T_a} \end{cases} \tag{3}$$

the flexural moment can be written as [11,20,27]:

$$M_p(t) = \frac{\psi}{6+\psi} E_a c T_a T_b \Lambda(t) \tag{4}$$

The aim of this article is the identification of the optimal voltage distribution for damping modal vibrations. In this regard, the voltage $V(t)$ will always be the same for each PP and only its sign varies according to a step function (Figure 3). In this way, the effect of different voltage distributions can be compared to each other.

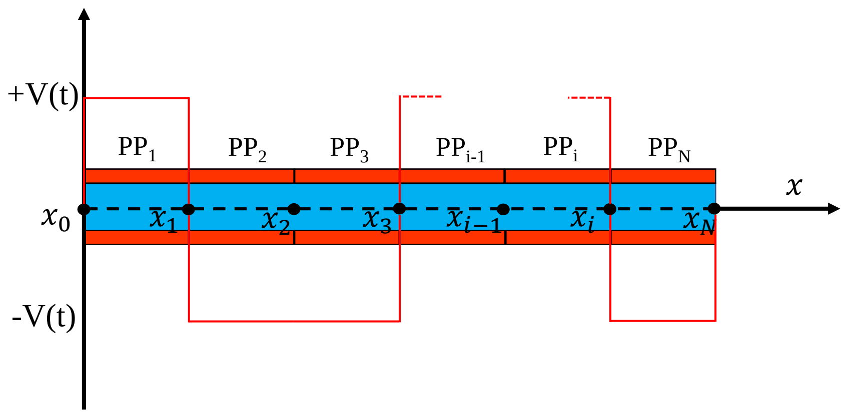

Figure 3. Example of a voltage distribution on the PPs.

The virtual work of the piezoelectric forces L_p can be written as:

$$\delta L_p = M_p \sum_{i=0}^{N_p-1} \left[\left(\frac{\partial \tilde{w}}{\partial x}|_{x=x_{i+1}} - \frac{\partial \tilde{w}}{\partial x}|_{x=x_i} \right) \delta(V_i) \right] \tag{5}$$

where N_p is the number of PPs, x_i are the points where there is a change of the voltage's sign, and the step function $\delta(V_i)$ may assume the values +1 or -1 depending on the plate i and the considered voltage distribution (see Figure 3). In this way, the assessment of the optimal voltage distribution lies in the search for the optimal points x_i where the voltage switches its sign. Let $w_j(x)$ be the generic vibration mode to be damped, the most effective voltage distribution will be the one that maximizes δL_p. Since M_p is constant for each PP, the variation of the work δL_p will depend essentially on the differences $\left(\frac{\partial \tilde{w}_j}{\partial x}|_{x=x_{i+1}} - \frac{\partial \tilde{w}_j}{\partial x}|_{x=x_i} \right)$, as a function of the different voltage distributions. This implies that it will be convenient to choose x_{i+1} and x_i at the extrema of the eigenmode's first derivative to maximize such difference. However, it will also be necessary to change the voltage's sign at each extremum in order to cumulate all the contributions and achieve the maximum damping effectiveness (Figure 4).

Thereby, the optimal voltage distribution will be obtained by changing the sign of $V(t)$ at each minimum or maximum of the eigenmode's first derivative that has to be dampened. The following formula can be used for all the considered boundary conditions to calculate the total virtual work of the piezoelectric forces:

$$\delta L_p = M_p \left[w'(x_L) - w'(x_0) + 2 \sum_{i=1}^{k} \left(w'(x_{2i-1}) - w'(x_{2i}) \right) \right] \tag{6}$$

with k being a parameter that depends on the number of the extrema points (N_e) that appear in w'· k can be found as follows:

$$k = \begin{cases} \frac{N_e - 1}{2} & \text{if there is not a maximum in } x = L \\ \frac{N_e - 2}{2} & \text{if there is a maximum in } x = L \end{cases} \tag{7}$$

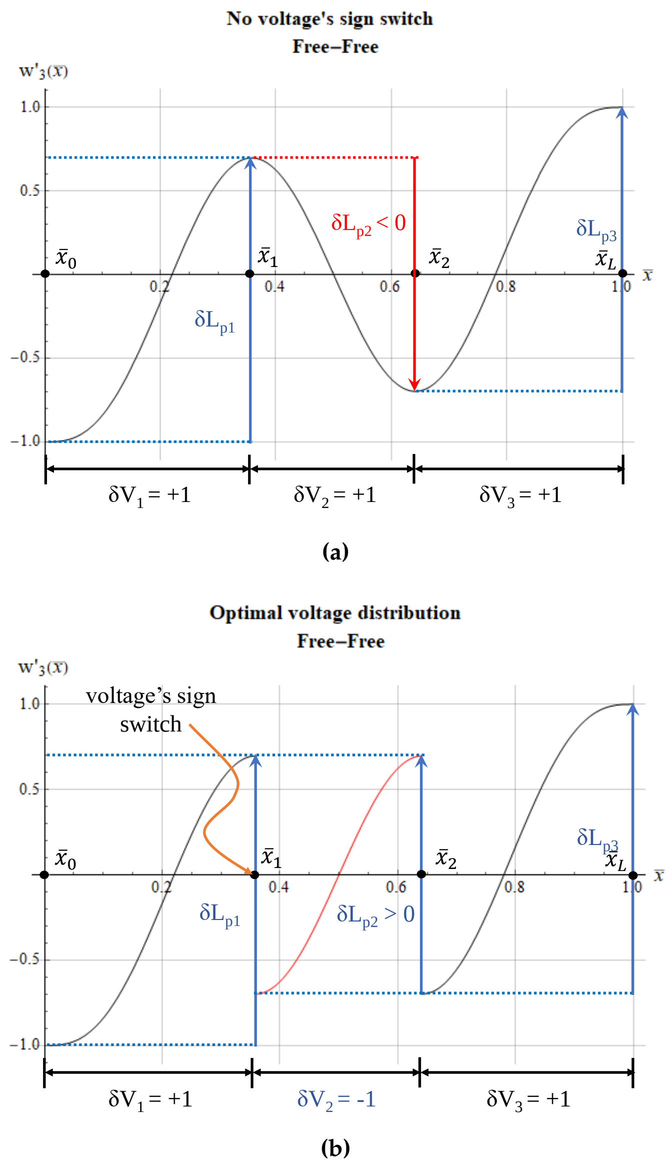

Figure 4. Example of the optimal voltage distribution to achieve the maximum work δL_p for the third mode and free-free boundary condition. δL_p is only dependent on the first derivative of the eigenmode ($w_3'(\bar{x})$): (**a**) no voltage's sign switch is provided, (**b**) optimal voltage distribution (two sign switches entailed). In the case (**a**), the total work $\delta L_p = \delta L_{p1} + \delta L_{p2} + \delta L_{p3}$ is not the highest since the work δL_{p2} is negative and reduces the total work. Case (**b**) shows that the optimal voltage distribution entails two voltage sign switches, respectively, at $\bar{x}_1 = 0.36$ and $\bar{x}_2 = 0.64$. In this way, the resulting total work $\delta L_p^{max} = \delta L_{p1} + \delta L_{p2} + \delta L_{p3}$ is the highest since δL_{p2} is actually positive. The solid red line represents the function $w_3'(\bar{x})$ when the voltage's sign is switched for $0.36 \leq \bar{x} \leq 0.64$.

3. Numerical Model and Results

A commercial multiphysics FEM code (*COMSOL*) was used to verify the analytical results on the optimal voltage distribution for several cases of beam constraints. The model geometry specifications are listed in Table 1.

Table 1. Geometric details of the beam and each PZT actuator.

beam	L (mm)	b (mm)	h_b (mm)
	300	30	3
PZT	L_p (mm)	b_p (mm)	h_p (mm)
	30	30	0.3

The beam is entirely covered by 10 PZT actuator couples, hence 2^{10} possible voltage distributions exist (Table 2) and they all are explored in order to assess the optimal one. The optimal voltage distribution is numerically evaluated by comparing the amplitudes of the displacement reached by a reference point for all the voltage distributions (with the only restriction of not selecting a node, i.e., zero-displacement point). Then, the voltage distribution that allows to obtain the maximum displacement is identified. The PZT and beam material specifications are reported in Table 3. For each considered boundary condition, the frequency response of the beam was simulated by supplying all the PPs with the harmonic voltage $V(t) = Ve^{j\omega t}$, where V is the voltage amplitude (set to 100 V), j is the imaginary unit, and ω is the angular frequency corresponding to one of the first three eigenmodes. The sign of the voltage has been distributed as reported in Table 2, so 1024 frequency response simulations have been performed for each eigenmode. The beam coupled with 10 PPs is modelled in a 3D environment and its mesh consists approximately of 50,000 free-triangular elements. The edges of each PZT actuator have been refined to enhance the solution's accuracy, since the piezoelectric moment provided by every PP is concentrated at the ends of each actuator (Section 2).

Table 2. Possible voltage distributions.

Distribution\PP	**1**	**2**	**3**	**4**	**5**	**6**	**7**	**8**	**9**	**10**
1	+1	+1	+1	+1	+1	+1	+1	+1	+1	+1
2	+1	+1	+1	+1	+1	+1	+1	+1	+1	−1
3	+1	+1	+1	+1	+1	+1	+1	+1	-	+1
4	+1	+1	+1	+1	+1	+1	+1	−1	+1	+1
5	+1	+1	+1	+1	+1	+1	−1	+1	+1	+1
...	...	...	...	...	...	...	...	...	...	...
k	+1	−1	+1	−1	−1	+1	−1	+1	+1	−1
...	...	...	...	...	...	...	...	...	...	...
$2^{10} = 1024$	−1	−1	−1	−1	−1	−1	−1	−1	−1	−1

Table 3. PZT actuators and beam material specifications.

Label	**Material**	**Density (kg/m^3)**	**Young's Modulus (GPa)**	**Poisson's Ratio**	$d_{31}(10^{-12}C/N)$
Beam	Aluminium	2700	70	0.3	–
Actuator	PZT-5A	7750	39	–	374

Figure 5 reports the comparison between the analytical and numerical calculated optimal voltage distribution considering the free-free boundary condition and the first three eigenmodes. As described in Section 2, the optimal voltage distribution provides a sign change whether a minimum or a maximum in the first derivative of the mode is encountered. When the first mode is excited, the best voltage distribution implies no sign change (Figure 5a). If the second mode has to be dampened, the voltage's sign must change from $\bar{x} = 0.5$ onwards (Figure 5b). When the third mode is excited, the most effective voltage distribution entails two voltage's sign changes, respectively, within $0 \leq \bar{x} \leq 0.36$ and $0.64 \leq \bar{x} \leq 1$ (Figure 5c). In this case, the FEM sign switch location are slightly shifted with respect to the extrema locations of $w'_3(\bar{x})$ because of the numerical discretization error. This is due to the inherent finite number of PZT plates; the edge of a PZT pair does not always coincide with an extremum of $w'_j(\bar{x})$. Figure 6 depicts the errors in the damping effectiveness to show the above mentioned considerations. In this case, the total analytical virtual work $\delta L_{p,an} = |\delta L_{p1,an}| + |\delta L_{p2,an}| + |\delta L_{p3,an}|$ is the maximum work theoretically achievable. Since 10 PZT actuator pairs are considered in the FEM simulations, the total virtual work obtained via FEM will be always lower than $\delta L_{p,an}$. $\delta L_{p,fem}$ and it can be written as $\delta L_{p,fem} = |\delta L_{p1,fem}| + |\delta L_{p2,fem}| + |\delta L_{p3,fem}| \leq \delta L_{p,an}$. The total damping effectiveness error due to the number of actuators can be written as $e_{tot} = e_1 + e_2$. The terms e_1 and e_2 can be calculated as $e_1 = \delta L_{p1,an} - \delta L_{p1,fem}$ and $e_2 = \delta L_{p3,an} - \delta L_{p3,fem}$. It is worth noting that $\delta L_{p2,an} - \delta L_{p2,fem} = e_1 + e_2$. The total percentage loss of damping due to the discretization can be written as:

$$e(\%) = \frac{\delta L_{p,an} - \delta L_{p,fem}}{\delta L_{p,an}} \tag{8}$$

For the considered cases, $e(\%)$ is always lower than 4–5% while, in the worst case (Figure 6), the discretization error yields to a numerical loss of damping effectiveness equal to 8%.

A similar fair agreement among the analytical and numerical outcomes can be observed for the fixed-fixed boundary condition (Figure 7). If the first mode is excited, the optimal voltage distribution entails two sign switches ($\bar{x} = 0.23$ and $\bar{x} = 0.77$), as reported in Figure 7a. The optimal voltage distribution to damp the second mode excitation includes three sign changes (Figure 7b), while four sign switches must be provided when the third eigenmode is excited (Figure 7c).

The numerical optimal voltage distributions for the first three modes of a pinned-pinned beam (Figure 8) are similar to those of the free-free beam modes (Figure 5). This is due to the fact that the ends of the beam are free to rotate for both boundary conditions. However, the local minima and maxima of $w'_j\bar{x}$ share the same absolute value in the case of pinned-pinned beams (Figure 8), while this is not the case for the free-free and fixed-fixed boundary conditions.

Finally, it seems to be confirmed that the proposed method allows to theoretically find the optimal voltage distribution on PZT actuator pairs, regardless of the boundary condition, which also ensures the highest achievable piezoelectric work δL_p. In other terms, by maximizing the piezoelectric work, the maximum damping efficiency can be achieved in the case of resonance mitigation.

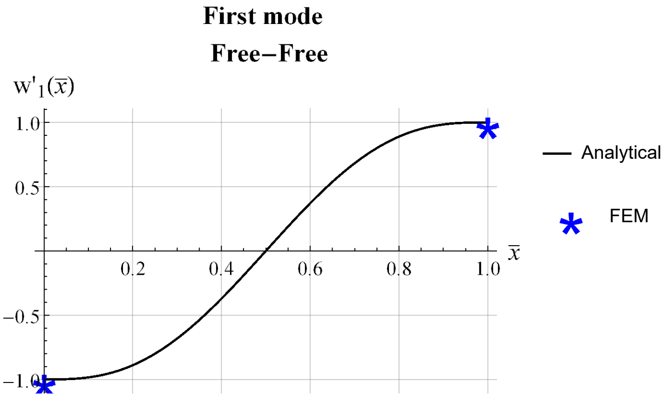

(a)

Figure 5. *Cont.*

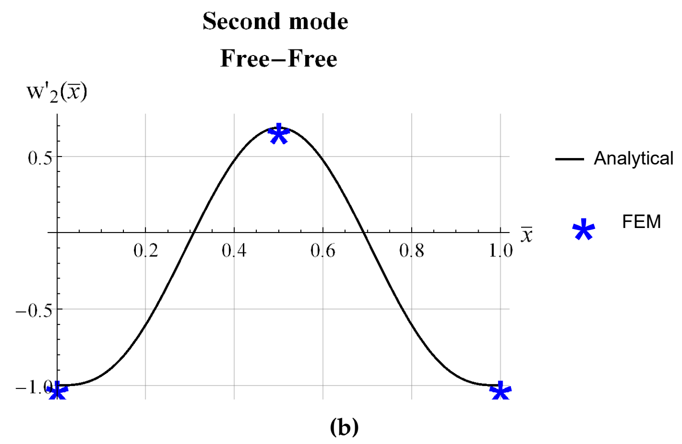

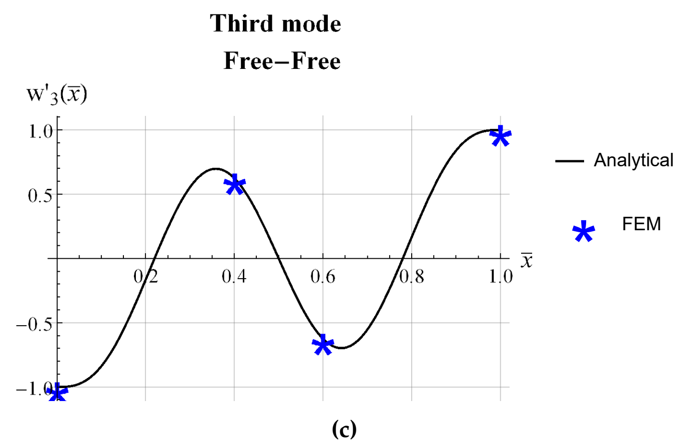

Figure 5. First derivatives of the first three modes for free-free boundary condition: (**a**) first mode, (**b**) second mode, and (**c**) third mode. The FEM results highlight the optimal location of the voltage sign switch (illustrated with blue stars).

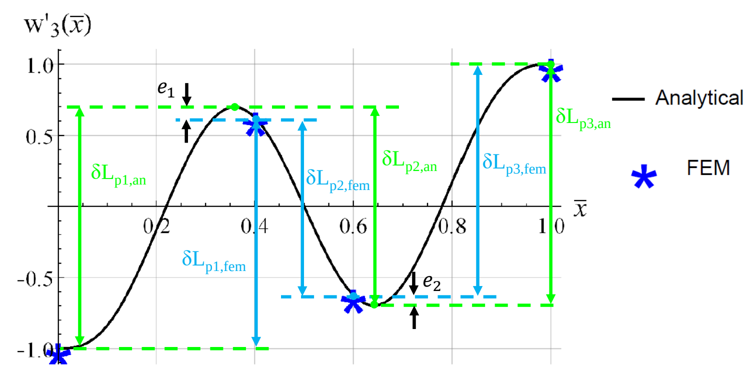

Figure 6. Example of discretization errors when evaluating the damping effectiveness in the case of free-free boundary conditions and third mode excitation. The total analytical virtual work $\delta L_{p,an} = |\delta L_{p1,an}| + |\delta L_{p2,an}| + |\delta L_{p3,an}|$ is the maximum theoretically achievable. Since 10 PZT actuator pairs are considered in the FEM simulations, the total virtual work, obtained via FEM, will be always lower than $\delta L_{p,an}$ and it can be written as: $\delta L_{p,fem} = |\delta L_{p1,fem}| + |\delta L_{p2,fem}| + |\delta L_{p3,fem}| \leq \delta L_{p,an}$. e_1 and e_2 can be obtained as: $e_1 = \delta L_{p1,an} - \delta L_{p1,fem}$ and $e_2 = \delta L_{p3,an} - \delta L_{p3,fem}$. It is worth noting that $\delta L_{p2,an} - \delta L_{p2,fem} = e_1 + e_2$. The total percentage loss of damping due to the discretization error (Equation (8)) is $e(\%) = \frac{\delta L_{p,an} - \delta L_{p,fem}}{\delta L_{p,an}} = \frac{2e_1 + 2e_2}{\delta L_{p,an}} = 8\%$.

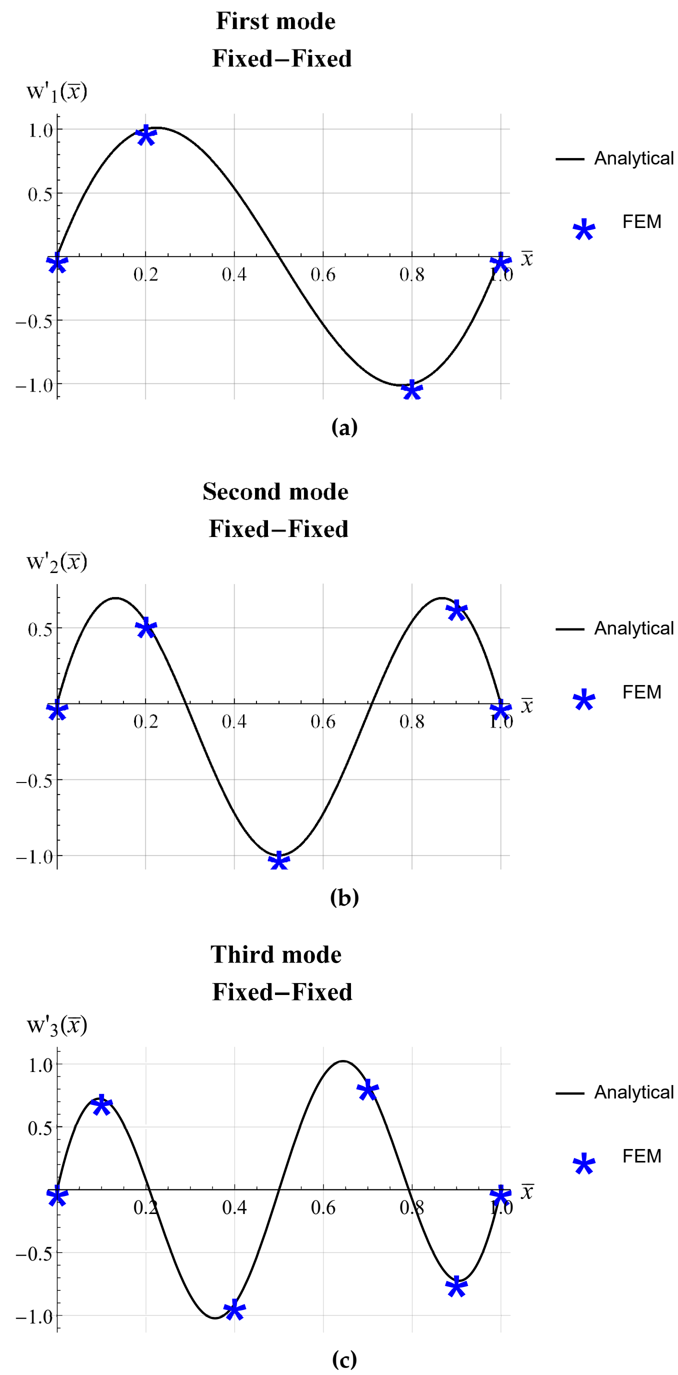

Figure 7. First derivatives of the first three modes for fixed-fixed boundary condition: (**a**) first mode, (**b**) second mode, and (**c**) third mode. The FEM results highlight the optimal location of the voltage sign switch (illustrated with blue stars).

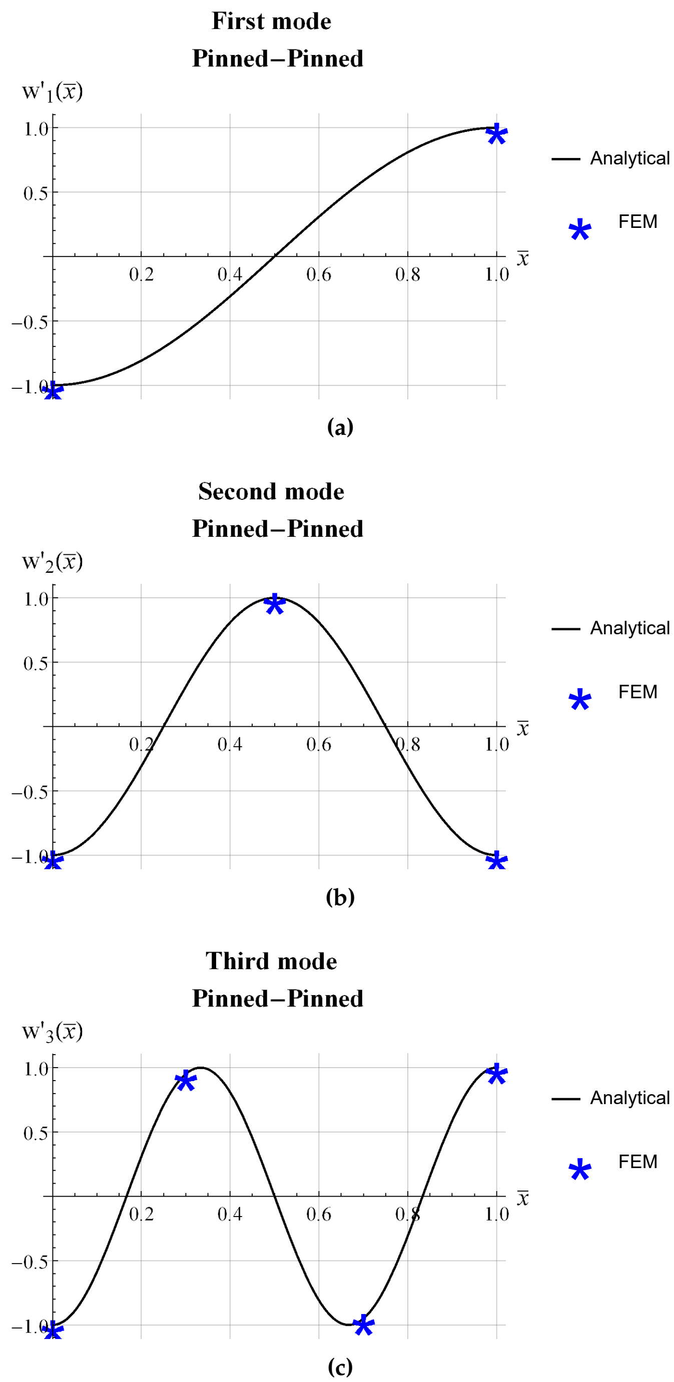

Figure 8. First derivatives of the first three modes for pinned-pinned boundary condition: (**a**) first mode, (**b**) second mode, and (**c**) third mode. The FEM results highlight the optimal location of the voltage sign switch (illustrated with blue stars).

In Figure 9a–d the damping effectiveness of several voltage distributions reported in Table 4 are compared in the case of the resonance induced by an external load $F(t)$. The load $F(t) = F_0 \cos(\omega_1 t)$ is evenly distributed on the beam length, with $F_0 = 15$ N and ω_1 being the angular frequency. The damping efficacy is calculated by considering the displacement of a reference point located at $\bar{x} = 0.2$ and driving the PPs with the same voltage amplitude $V = 80$ V for each considered voltage distribution. It is worth noting that when the PPs within the maximum and minimum of the first derivative of the first eigenmode is not activated at all (i.e., $\delta V_i = 0$, Equation (5)), about 50% damping effectiveness can be reached

(Figure 9a). In this case, the virtual work of the piezoelectric forces is not optimized since the participation of PPs located between $\bar{x}$ =0.2 and $\bar{x}$ =0.8 is zero. Such a contribution can be recovered, reaching 100% damping efficacy by switching the sign of the voltage at $\bar{x}$ =0.2, and proving the validity of the proposed method (Figure 9c). In fact, considering Figure 10, the total piezoelectric virtual work δL_{ptot} can be written as:

$$\delta L_{ptot} = \delta L_{p1} + \delta L_{p2} + \delta L_{p3} \tag{9}$$

which can be normalized to highlight the individual percentage contributions:

$$r_{tot} = r_1 + r_2 + r_3 = \frac{\delta L_{p1}}{\delta L_{ptot}} + \frac{\delta L_{p2}}{\delta L_{ptot}} + \frac{\delta L_{p3}}{\delta L_{ptot}} = 1 \tag{10}$$

Since the difference between the damping efficacy obtained with A and OVD_1 distributions is 50%, it can be seen that it actually coincides with r_2 because $r_1 + r_3 = 50\%$. When the optimal voltage distribution for the second eigenmode excitation (OVD_2) and B distribution are activated, the damping efficacy is way lower than that reached with the OVD_1 (Figure 9b–d).

Table 4. Selected voltage distributions for the damping effectiveness comparison illustrated in Figure 9 and considering the first eigenmode excitation of the fixed-fixed beam. OVD_1 and OVD_2 are the optimal voltage distributions when the mode is excited, respectively, for the first and the second mode.

Distribution\PP	1	2	3	4	5	6	7	8	9	10
A	+1	+1	0	0	0	0	0	0	+1	+1
B	+1	+1	−1	−1	−1	+1	+1	−1	−1	+1
OVD_1	+1	+1	−1	−1	−1	−1	−1	−1	+1	+1
OVD_2	+1	+1	−1	−1	−1	+1	+1	+1	+1	−1

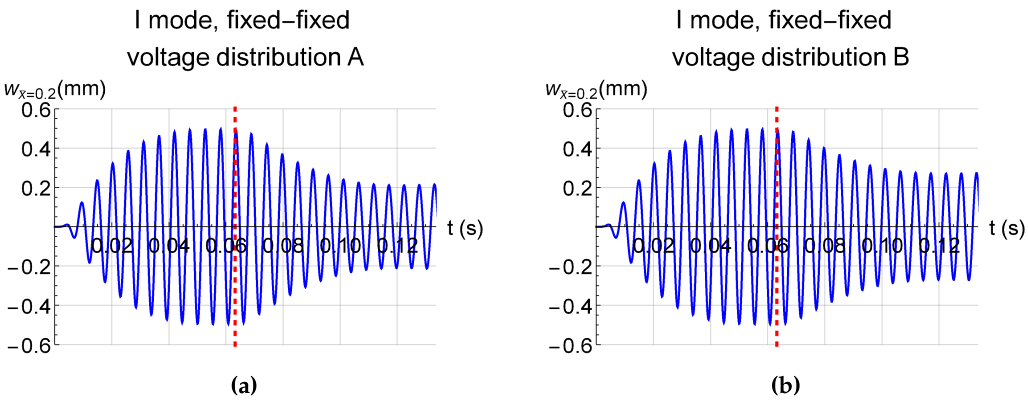

Figure 9. *Cont.*

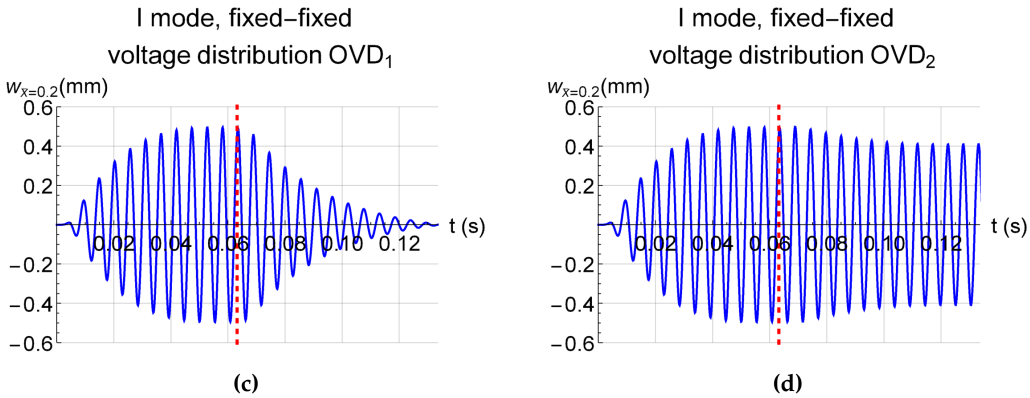

Figure 9. Example of the damping efficacy achieved activating the voltage distributions listed in Table 4. $w_{\bar{x}=0.2}$ vs. time plots in the case of: (**a**) activation of the voltage distribution A, (**b**) activation of the voltage distribution B, (**c**) activation of the voltage distribution OVD_2, and (**d**) activation of the voltage distribution OVD_1. The first eigenmode of the fixed-fixed beam is excited by the external load $F(t)$, evenly distributed on the beam length, with $F(t) = F_0 \cos(\omega_1 t)$, $F_0 = 15$ N and ω_1 being the angular frequency of the first mode (1174.4 rad/s). The vertical displacement of a point located at $\bar{x} = 0.2$ is used as the reference point. The dashed red line shows the instant of voltage distribution activation.

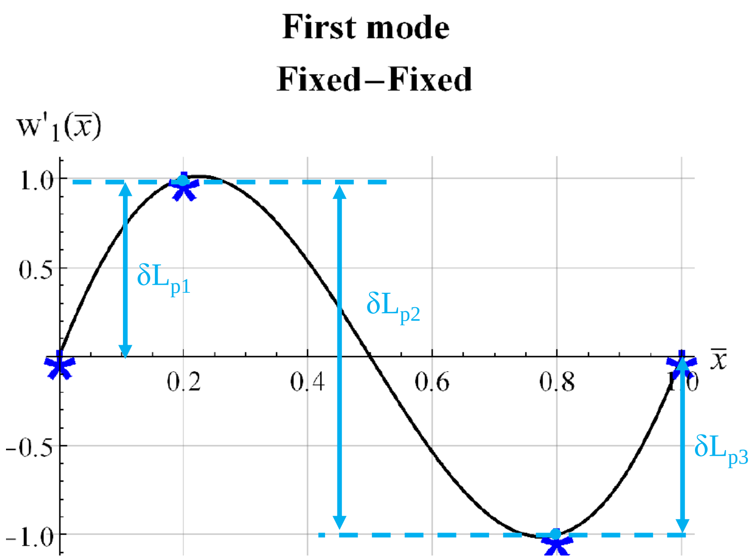

Figure 10. Virtual works of the piezoelectric forces (δL_p) in the case of the first eigenmode excitation in a fixed-fixed beam. The FEM results highlight the optimal location of the voltage sign switch (illustrated with blue stars).

4. Conclusions

The optimal voltage distribution to dampen the vibration at resonance has been investigated for the Euler–Bernoulli beam entirely covered with PZT actuator pairs and for different boundary conditions. The optimization method lies in the maximization of the virtual work of the piezoelectric forces that depends on the first derivative of the target mode shape. The optimal voltage distributions have been investigated for the first three eigenmodes and free-free, fixed-fixed, and pinned-pinned boundary conditions. It was numerically verified that the voltage must change its sign whenever a minimum or maximum of the piezoelectric work is reached. The numerical simulations have been performed through a FEM code considering 10 PZT actuator pairs and a fair agreement with the theoretical predictions arises for each case under study. The proposed approach may be relevant for many engineering problems involving the design of active vibration damping systems, based on the PZT actuators.

Author Contributions: Conceptualization, A.R. and F.B.; methodology, A.R. and F.B.; software, F.B.; validation, A.R. and F.B.; formal analysis, F.B.; investigation, A.R. and F.B.; data curation, A.R.; writing—original draft preparation, A.R. and F.B.; writing—review and editing, A.R. and F.B.; visualization, A.R.; supervision, F.B. All authors have read and agreed to the published version of the manuscript.

Funding: This research received no external funding.

Institutional Review Board Statement: Not applicable.

Informed Consent Statement: Not applicable.

Data Availability Statement: Not applicable.

Conflicts of Interest: The authors declare no conflict of interest.

Nomenclature

L	beam's length
d_{31}	piezoelectric coefficient
ρ	beam's density
E_a	Young's modulus of the piezoelectric actuator
E_b	Young's modulus of the beam
M_p	piezoelectric bending moment
T_a	piezoelectric actuator thickness
T_b	beam's thickness
b	beam's width
A	beam's cross-section area
w	vertical displacement
$\widetilde{w}$	virtual vertical displacement
$w_i(x)$	i-th flexural mode of the cantilever beam
$\bar{x}$	dimensionless length of the beam: $\frac{x}{L_b}$
x_i	points where the potential changes its sign
$\bar{x} = \frac{x}{L}$	dimensionless length
$'$	derivative with respect to the $x-$axis

References

1. Tamer, O.; Walter, F.; Sinapius, M.; Böl, M. A Computational Geometric Parameter Optimization of the Thermomechanical Deicing Concept. *Actuators* **2022**, *11*, 223. [CrossRef]
2. Shamim, M.B.; Hörsting, M.; Wulfinghoff, S. Variational Reduced-Order Modeling of Thermomechanical Shape Memory Alloy Based Cooperative Bistable Microactuators. *Actuators* **2023**, *12*, 36. [CrossRef]
3. Nguyen, Q.A.; Jorgensen, S.; Ho, J.; Sentis, L. Characterization and Testing of an Electrorheological Fluid Valve for Control of ERF Actuators. *Actuators* **2015**, *4*, 135–155. [CrossRef]
4. Oh, J.S.; Sohn, J.W.; Choi, S.B. Applications of Magnetorheological Fluid Actuator to Multi-DOF Systems: State-of-the-Art from 2015 to 2021. *Actuators* **2022**, *11*, 44. [CrossRef]
5. Jeniš, F.; Kubík, M.; Michálek, T.; Strecker, Z.; Žáček, J.; Mazůrek, I. Effect of the Magnetorheological Damper Dynamic Behaviour on the Rail Vehicle Comfort: Hardware-in-the-Loop Simulation. *Actuators* **2023**, *12*, 47. [CrossRef]
6. Kang, M.G.; Jung, W.S.; Kang, C.Y.; Yoon, S.J. Recent Progress on PZT Based Piezoelectric Energy Harvesting Technologies. *Actuators* **2016**, *5*, 5. [CrossRef]
7. Aabid, A.; Parveez, B.; Raheman, M.A.; Ibrahim, Y.E.; Anjum, A.; Hrairi, M.; Parveen, N.; Zayan, J.M. A Review of Piezoelectric Material-Based Structural Control and Health Monitoring Techniques for Engineering Structures: Challenges and Opportunities. *Actuators* **2021**, *10*, 101. [CrossRef]
8. Harti, K.E.; Rahmoune, M.; Sanbi, M.; Saadani, R.; Bentaleb, M.; Rahmoune, M. Finite Element Model of Vibration Control for an Exponential Functionally Graded Timoshenko Beam with Distributed Piezoelectric Sensor/Actuator. *Actuators* **2019**, *8*, 19. [CrossRef]
9. Barrett-Gonzalez, R.; Wolf, N. High Speed Microactuators for Low Aspect Ratio High Speed Micro Aircraft Surfaces. *Actuators* **2021**, *10*, 265. [CrossRef]

10. Barrett-Gonzalez, R.; Wolf, N. High-Rate, High-Precision Wing Twist Actuation for Drone, Missile, and Munition Flight Control. *Actuators* **2022**, *11*, 239. [CrossRef]
11. Botta, F.; Rossi, A.; Belfiore, N.P. A novel method to fully suppress single and bi-modal excitations due to the support vibration by means of piezoelectric actuators. *J. Sound Vib.* **2021**, *510*, 116260. [CrossRef]
12. Botta, F.; Toccaceli, F. Piezoelectric Plates Distribution for Active Control of Torsional Vibrations. *Actuators* **2018**, *7*, 23. [CrossRef]
13. Botta, F.; Rossi, A. Introductory PZT actuators optimal working configuration experimental study in a turbofan engine fan rotor blade. In Proceedings of the Turbo Expo: Power for Land, Sea, and Air, Online, 21–25 September 2020; American Society of Mechanical Engineers: New York, NY, USA, 2020; Volume 84232, p. V011T30A035.
14. Mokrani, B.; Bastaits, R.; Romanescu, I.; Horodinca, M.; Burda, I.; Preumont, A. Passive Damping of Rotationally Periodic Structures with Tuned Piezoelectric Inductive Shunt. *Actuators* **2018**, *7*, 41. [CrossRef]
15. Rossi, A.; Botta, F.; Giovannelli, A.; Belfiore, N.P. High efficiency active damping on a fan rotor blade in case of resonant vibrations by means of piezoelectric actuators. In Proceedings of the ASME Turbo Expo 2021: Turbomachinery Technical Conference and Exposition, GT 2021, Online, 7–11 June 2021; Volume 9A-2021. [CrossRef]
16. Goltz, I.; Böhmer, H.; Nollau, R.; Belz, J.; Grüber, B.; Seume, J. Piezo-Electric Actuation of Rotor Blades in an Axial Compressor. In Proceedings of the ETC 2009—8th European Conference on Turbomachinery, Graz, Austria, 23–27 March 2009.
17. Provenza, A.J.; Morrison, C.R. Control of Fan Blade Vibrations Using Piezoelectrics and Bi-Directional Telemetry. In Proceedings of the ASME 2011 Turbo Expo: Turbine Technical Conference and Exposition, Vancouver, BC, Canada, 6–10 June 2011; American Society of Mechanical Engineers Digital Collection: New York, NY, USA, 2011; pp. 923–930.
18. Choi, B.; Kauffman, J.; Duffy, K.; Provenza, A.; Morrison, C. Active vibration reduction of titanium alloy fan blades (FAN1) using piezoelectric materials. *NASA/TM* **2010**, *2010*, 216335.
19. Rossi, A.; Botta, F.; Giovannelli, A.; Belfiore, N.P. A novel approach to reduce fan rotor blades stress in case of resonance due to inlet flow distortion by means of piezoelectric actuators. *J. Sound Vib.* **2023**, *548*, 117552. [CrossRef]
20. Crawley, E.F.; De Luis, J. Use of piezoelectric actuators as elements of intelligent structures. *AIAA J.* **1987**, *25*, 1373–1385. [CrossRef]
21. Ducarne, J.; Thomas, O.; Deü, J. Placement and dimension optimization of shunted piezoelectric patches for vibration reduction. *J. Sound Vib.* **2012**, *331*, 3286–3303. [CrossRef]
22. Barboni, R.; Mannini, A.; Fantini, E.; Gaudenzi, P. Optimal placement of PZT actuators for the control of beam dynamics. *Smart Mater. Struct.* **2000**, *9*, 110. [CrossRef]
23. Gupta, V.; Sharma, M.; Thakur, N. Optimization Criteria for Optimal Placement of Piezoelectric Sensors and Actuators on a Smart Structure: A Technical Review. *J. Intell. Mater. Syst. Struct.* **2010**, *21*, 1227–1243. [CrossRef]
24. Botta, F.; Dini, D.; Schwingshackl, C.; di Mare, L.; Cerri, G. Optimal Placement of Piezoelectric Plates to Control Multimode Vibrations of a Beam. *Adv. Acoust. Vib.* **2013**, *2013*, 905160. [CrossRef]
25. Botta, F.; Rossi, A.; Schinaia, L.; Scorza, A.; Orsini, F.; Sciuto, S.; Belfiore, N. Experimental validation on optimal placement of pzt plates for active beam multimode vibrations reduction. In Proceedings of the AIMETA 2017 Proceedings of the 23rd Conference of the Italian Association of Theoretical and Applied Mechanics, Salerno, Italy, 4–7 September 2017; Volume 3, pp. 2258–2269.
26. Rossi, A.; Botta, F.; Maiozzi, R.; Scorza, A.; Sciuto, S.A. Experimental results for active control of multimodal vibrations by optimally placed piezoelectric actuators. *MATEC Web Conf.* **2018**, *211*, 20001. [CrossRef]
27. Botta, F.; Scorza, A.; Rossi, A. Optimal Piezoelectric Potential Distribution for Controlling Multimode Vibrations. *Appl. Sci.* **2018**, *8*, 551. [CrossRef]
28. Cross, R. Factors affecting the vibration of tennis racquets. *Sport. Eng.* **2015**, *18*, 135–147. [CrossRef]
29. Brody, H. Models of baseball bats. *Am. J. Phys.* **1990**, *58*, 756–758. [CrossRef]
30. Vigneshwaran, K.; Behera, R.K. Vibration Analysis of a Simply Supported Beam with Multiple Breathing Cracks. *Procedia Eng.* **2014**, *86*, 835–842. [CrossRef]